Principles and Properties of RNA Self-Assembly

Gabriel Tauber
Department of Molecular, Cellular, and Developmental Biology
University of Colorado Boulder

Defense Date: April 9, 2019

Thesis Advisor: Roy Parker, PhD, Howard Hughes Medical Institute and Department of Biochemistry

Committee Member: Tom Cech, PhD, Howard Hughes Medical Institute and Department of Biochemistry

Honors Representative: Brian DeDecker, PhD, Department of Molecular, Cellular, and Developmental Biology

Abstract

Ribonucleoprotein (RNP) granules are membraneless assemblies of condensed RNA and protein that form through multivalent interactions between the constituent components. Recently, RNA self-assembly has been shown to contribute to the formation of stress granules, which are RNP granules associated with the stress response and neurodegeneration. However, little is understood about the properties of self-assembled RNA. Here, I show that different RNA sequences can self-assemble into condensates with distinct material properties and partitioning preferences *in vitro*. Due to interactions that minimize surface free energy, RNA self-assembly can generate the spontaneous self-patterning of RNA assemblies. By reducing surface free energy, thereby promoting RNA-RNA interactions, RNAs stabilize multiphase RNA assemblies or assemble into surface shells composed of a hyperstable interacting meshwork of RNA. In principle, the thermostability of RNA self-assembly could give rise to uncontrolled RNA aggregation in the cell without modulatory mechanisms, and I show that the condensation of certain transcripts onto stress granules can be limited by the DEAD-box helicase eIF4A and potentially other helicases. These data suggest a view of the cell where intermolecular RNA-RNA interactions drive RNA self-assembly and where the cell utilizes a diversity of mechanisms to limit such RNA based condensation.

Introduction

Ribonucleoprotein (RNP) granules, like stress granules (SGs), nuclear paraspeckles, and nucleoli, are membraneless compartments composed of RNA and protein. There is a diversity of RNP granules in the cell, and RNP granules are involved with viral infection and are associated with numerous neurodegenerative diseases (Protter and Parker, 2016; Banani *et al*., 2017; Shin and Brangwynne, 2018). It is commonly thought that RNP granules may form through multivalent protein-protein interactions between intrinsically disordered regions (Boeynaems *et al*., 2018).

Recently, evidence has emerged that intermolecular RNA-RNA interactions are important to SG formation. For instance, SGs require a pool of non-translating RNA to appear (Protter and Parker, 2016), and they can be induced by injection of RNA into puromycin-treated cells (Bounedjah *et al*., 2014), demonstrating that elevated non-translating RNA concentrations promote SG formation. Moreover, protein-free total RNA extracts readily self-assemble in physiological salt, pH, and polyamine conditions *in vitro* at modest RNA concentrations, and the self-assembled RNAs recapitulate the SG transcriptome (Van Treeck *et al*., 2018), implicating a shared physical basis in how the RNA self-assembles *in vitro* and how it condenses into SGs.

Roles for RNA in forming, maintaining, and organizing RNP granules and similar condensates are not limited to SGs. For example, nuclear paraspeckles require the lncRNA *NEAT1* to form (Fox and Lamond, 2010), and *NEAT1* regions organize paraspeckles with a core-shell morphology (West *et al*., 2016). The Barr body is formed when the lncRNA *XIST* coats the X chromosome, which then condenses (Creamer and Lawrence, 2017). In the *Drosophila* embryo, homotypic intermolecular base-pairing between *oskar* mRNAs or *bicoid* mRNAs determines which RNP granules the mRNAs will localize to, in the anterior or posterior, promoting polarity establishment (Van Treeck and Parker, 2018).

Little is understood about the physical properties of self-assembled RNA. In principle, multiple RNA molecules could interact through hydrogen bonding, π-π contacts between nucleobases, and/or Coulombic interactions between the phosphate backbone and cations like polyamines. These interactions cover a range of strength and specificity and are dependent on the composition of the RNA; therefore, self-assembled RNA can exhibit different sequence- and structure-dependent material phases *in vitro*, including colloidal droplets, gels, and liquid crystals (Yevdokimov *et al*., 1992; Golo *et al*., 2001; Zanchetta *et al*., 2008; Aumiller and Keating, 2016; Aumiller *et al*., 2016; Banerjee *et al*., 2017; Van Treeck *et al*., 2018; Langdon *et al*., 2018). Increased *trans* nucleic interactions can lead to more stable assemblies (Vieregg *et al*., 2018), and condensates formed from different homopolymer RNAs demonstrate distinct material phases and viscosities (Yevdokimov *et al*., 1992; Van Treeck *et al*., 2018), with polypurines self-assembling into more viscous or gel-like structures than polypyrimidines. Furthermore, assemblies of polyU RNA and polyamines are able to concentrate peptides and antisense oligonucleotides inside their interiors and to assemble liposomes at their interfacial surfaces (Aumiller *et al*., 2016), illustrating the principle that RNA self-assemblies can recruit and organize a variety of biomolecules.

The diversity and relative ease of RNA self-assembly is consistent with RNA-based assemblies playing myriad cellular roles, but also creates a need for the cell to modulate the process. One possible cellular mechanism for limiting RNA self-assembly would be the activity of RNA chaperones like RNA helicases (Van Treeck and Parker, 2018), a class of ATPases which unwinds RNA-RNA interactions (Jarmoskaite and Russell, 2014) and could thereby dissolve or limit RNA self-assembly in the cell. Notably, a wide variety of RNP granules contain RNA helicases (Dias *et al.*, 2010; Calo *et al*., 2015; Jain *et al*., 2016; Hubstenberger *et al*., 2017), and these are often conserved across eukaryotes (Linder and Fuller-Pace, 2013; Jarmoskaite and Russell, 2014). For example, SGs contain helicase proteins like Ded1/DDX3 and Tif1/eIF4A (Jain *et al*., 2016) and P bodies (another RNP granule type) contain the helicase Dhh1/DDX6 in both yeast and mammals (Anderson and Kedersha, 2006; Sheth and Parker, 2007). Consistent with the hypothesis that RNA helicases modulate the RNA self-assembly state of the cell, mutations in the ATPase core of Dhh1 lead to the formation of constitutive P bodies that trap RNA and display reduced dynamics in yeast (Mugler *et al*., 2016). Similarly, yeast Ded1 ATPase mutations promote persistent SGs (Hilliker *et al*., 2011), and mutations in the ATPase domain of the mammalian helicase RHAU lead to altered SG dynamics (Chalupnikova *et al*., 2008).

Here, I show that RNA sequence affects the formation and dynamics of RNA self-assemblies, and that different sequences can homotypically cluster, forming self-patterning networks. I also demonstrate that numerous RNAs can spontaneously assemble on the surfaces of RNA condensates and purified mammalian SGs, and that the intermolecular RNA-RNA interactions driving this are stabilized by reducing the surface free energy of the condensate. Finally, I show that the DEAD-box helicase eIF4A can influence the condensation of certain RNAs onto granules in cells, supporting a role for RNA helicases in modulating RNA self-assembly in the cell.

Results

Surface free energy and RNA-RNA interactions drive spontaneous patterning of RNA assembly

Different sequences of RNA have differential intermolecular interaction capacities which leads to distinct material properties in the self-assembled RNA (Van Treeck *et al*., 2018). To begin to assess how different sequences of RNA could partition into an RNA self-assembly, I made polyA, polyC, or polyU homopolymer self-assemblies (polyG forms stable aggregates in these conditions and was not tested) in the presence of each of five different fluorescent oligonucleotides with simple sequences: A_{19}, C_{19}, G_5, U_{19}, or PTR ($[UCUCUAAAAA]_5$; Figure 1A). As expected, the oligonucleotides antisense to the condensed homopolymers all partitioned robustly and homogeneously (Figure 1B). By contrast, the other oligonucleotides displayed different modes of recruitment including partitioning weakly and homogenously and being recruited into puncta or rings on the surfaces of the homopolymer droplets.

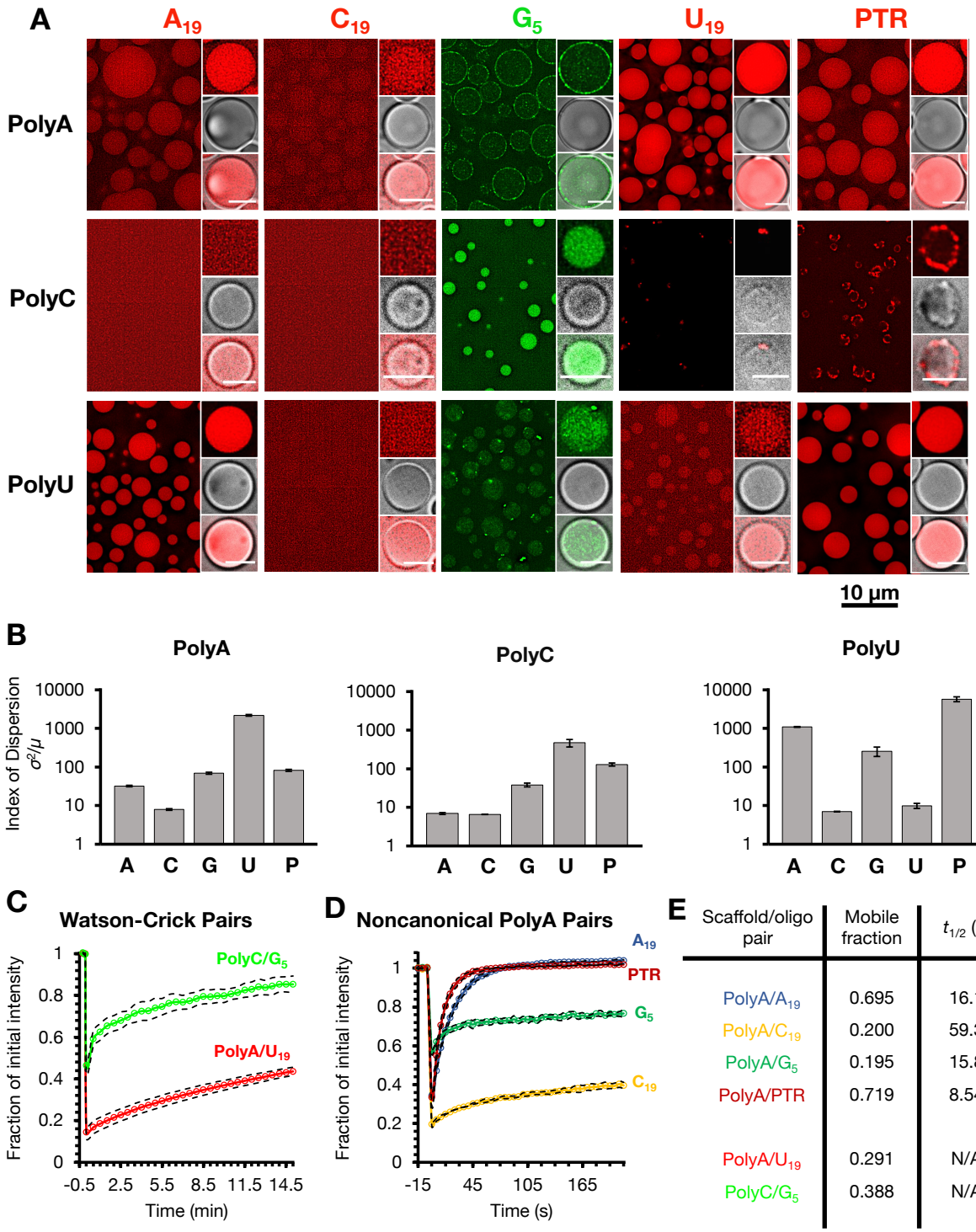

Figure 1. RNA sequence drives differential partitioning and dynamics in recruited RNA. **(A)** Pairwise combinations of long homopolymers and simple fluorescent oligos were condensed together and subsequently imaged. Contrast is not equally scaled. Large panel scale bars is 10 µm. Inset scale bars are 3 µm. **(B)** To assess how well each pairwise combination partitioned or organized an oligo, indices of dispersion were calculated for each condition, where the index of dispersion is a statistical measure of image inhomogeneity. Error bars represent 95% confidence intervals. **(C)** FRAP of polyC/G_5 and polyA/U_{19}. **(D)** PolyA droplets were incubated with the listed oligos, then subjected to FRAP. **(C-D)** Dashed lines represent ±1 standard deviation. **(E)** Table of calculated immobile fractions and $t_{1/2}$ times for the analyzed pairwise combinations.

These data reveal how different kinds of RNA-RNA interactions influence the recruitment of RNA to RNA condensates. In the first case, Watson-Crick interactions drive strong, homogeneous recruitment of oligos, as with the U_{19}/polyA combination.. In another case, certain RNA-RNA interactions, as with the C_{19}/polyC combination, do not enrich the oligonucleotides. By contrast, with some noncanonical pairs, such as C_{19}/polyA, the oligos weakly or moderately recruited, indicating that oligo-scaffold interactions are lower energy than oligo-solvent interactions. These data demonstrate that noncanonical intermolecular RNA-RNA interactions can promote dynamic partitioning to RNA condensates. Most intriguingly, some noncanonical oligo/scaffold combinations, like PTR/polyC, lead to enrichment of the oligonucleotide into rings or puncta on the surfaces of the RNA condensates, with strong partitioning. This indicates that for those pairs, the surface creates an energy well, disfavoring interactions in the interior of the condensate, while oligo-scaffold interactions appear more favorable than oligo-solvent interactions. Notably, the oligos that most robustly localize to surfaces, G_5 and PTR, have the potential to homotypically interact: G_5 could form G-quadruplexes and PTR's polypyrimidine tracts could interact with the A_5 linkers. It is probable that the surface promotes homotypic intermolecular interactions, further stabilizing the system (see below).

To assess the dynamics of oligonucleotide partitioning to homopolymer condensates, I performed fluorescence recovery after photobleaching (FRAP) on various pairwise combinations of homopolymer condensate scaffolds and fluorescent oligos. As expected, combinations facilitating Watson-Crick interactions led to very slow recovery following photobleaching (Figure 1C, Figure S1A) and relatively low mobile fractions (Figure 1E). In contrast, non-complementary oligos displayed a range of dynamics with polyA condensates (Figure 1D, Figure S1B). A_{19} and PTR displayed the highest mobile fractions and the quickest recoveries, indicating that the intermolecular interactions they form within the condensate are labile. By contrast, G_5 displayed the lowest mobile fraction, which would be consistent with the formation of stable G-quadruplex interactions within the surface puncta, immobilizing oligos. Surprisingly, C_{19} displayed the slowest kinetics of recovery, and had the second-lowest mobile fraction, implying that the oligo's accessibility to the polyA condensate is limited and that what little C_{19} does enrich in the droplets remains trapped. Notably, the immobility of an oligo did not appear to correlate with its partitioning, implying that labile intermolecular RNA-RNA interactions could potentially recruit and enrich RNAs in RNP granules.

To begin to assess how RNA sequence composition affects the self-assortment and material properties of RNA assemblies on a larger scale, I observed the co-assembly of pairwise combinations of homopolymer RNAs labeled by fluorescent antisense oligonucleotides. If interactions were very stable, they would drive the formation of stable assemblies containing both species. PolyA and polyU are complementary and this high degree of base-pairing drove the formation of gelatinous aggregates containing both homopolymers (Figure 2A). This is consistent with the slow recovery of U_{19} in polyA following photobleaching (Figure 1C, Figure S1A).

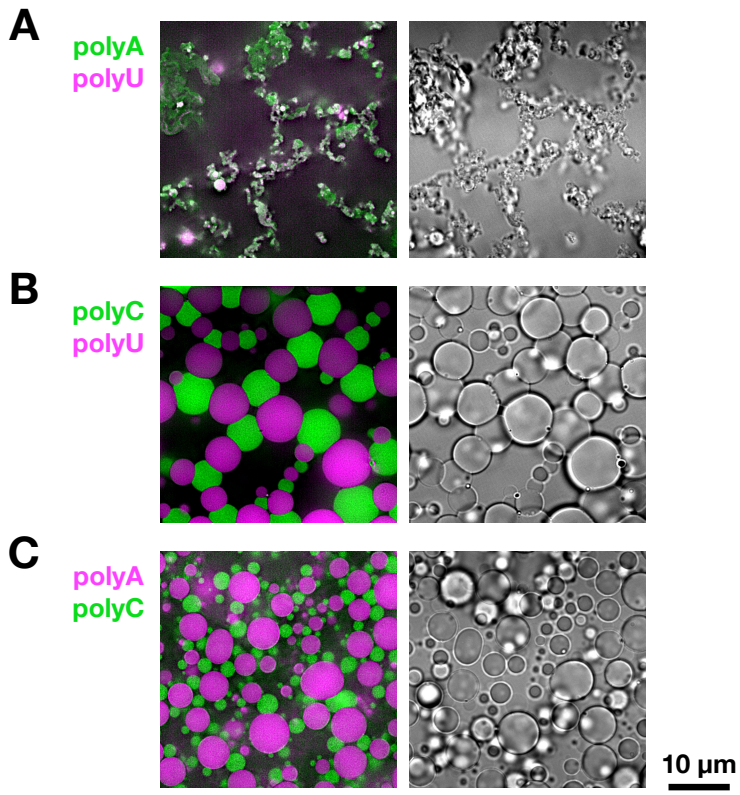

Figure 2. Homotypic interactions and surface free energy drive the spontaneous patterning of RNA self-assembly. **(A)** When mixed, polyA and polyU form stable, gelatinous aggregates, consistent with forming strong intermolecular interactions. **(B)** PolyC and polyU homotypically cluster, but remain associated at droplet interfaces, forming patterned networks. **(C)** PolyA and polyC also homotypically cluster and associate at surfaces, but are more flocculated. **(A-C)** Scale bar is 10 µm.

In contrast to strong interactions, weakly interacting homopolymers could conceivably co-assemble, assemble into separate condensates, or form multiphase assemblies. Strikingly, mixtures of polyC and polyU formed organized, branching networks of alternating and immiscible polyC and polyU droplets (Figure 2B). The polyC/polyU interface is elongated, deforming the droplets, indicating that the polyC/polyU interface is lower-energy than either homopolymer/solvent phase boundary, leading to more stable interactions between different RNA condensate surfaces. Similarly, polyA and polyC formed separate assemblies associated at surfaces (Figure 2C). These observations demonstrate the RNA condensates recruit other condensates, and presumably individual RNAs, to their surfaces, reducing the free energy of the system.

These data demonstrate that the strength of intermolecular RNA-RNA interactions can drive the formation of co-assemblies or separate, homotypic assemblies. Strong interactions like Watson-Crick interactions (Figure 2A) and G-quadruplexes (Van Treeck *et al*., 2018) give rise to stable, gel-like assemblies. Weakly interacting RNAs can form separate assemblies that interact at their interfaces (Figure 2B-C), which are stabilized over condensate-solvent interfaces, and this reduces the free energy of the system and induces the spontaneous patterning of self-assembled RNA. These data also indicate that, in condensation conditions, A:A and C:C interactions are favored over A:C interactions, and similarly, the summation of U:U and C:C interactions is more stable than if they were U:C interactions. Adenosine residues are in principle able to form more hydrogen bonds and π-π interactions than pyrimidines, but the occurrence of homotypic clustering with the polypyrimidines is more difficult to explain. Thus, the strengths of the different intermolecular RNA-RNA interactions control the material properties and organization of RNA self-assemblies.

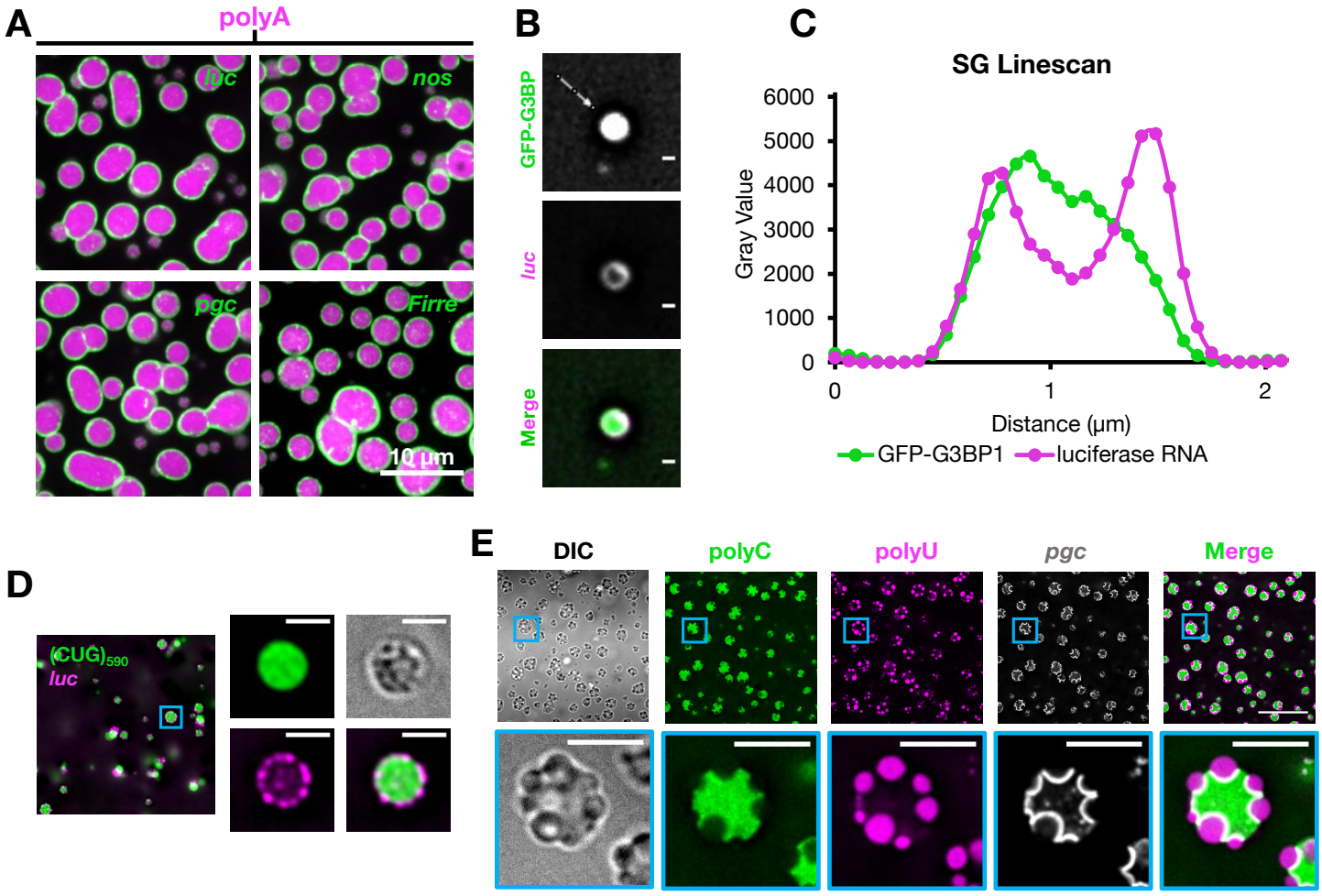

Figure 3. RNA condensates and stress granules recruit RNA to their interfaces. **(A)** PolyA (visualized by fluorescent U_{19}) RNA was condensed with the indicated fluorescent *in vitro* transcribed RNAs, which demonstrate robust surface localization. Scale bar is 10 μm. **(B-C)** SGs can recruit fluorescent RNAs to their surfaces. **(B)** Images of a SG, visualized by GFP-G3BP1, with surface-recruited RNA. The arrow in the top panel determines the linescan. Scale bars are 500 nm. **(C)** Linescan of the granule in (B). **(D)** A model fluorescent *in vitro* transcribed *DMPK* reRNA was condensed with other fluorescent *in vitro* transcripts, which show recruitment into puncta on the surface of the reRNA condensate. Inset scale bars are 2 μm. **(E)** Fluorescent *in vitro* transcribed *pgc* was condensed with antisense-labeled polyC and polyU, leading to multiphase assemblies with interfacial *pgc*. Inset scale bars are 5 μm.

Because surface oligonucleotide-RNA condensate and condensate-condensate interactions reduce the free energy of their respective systems, it should be favorable for RNA self-assemblies and RNP granules to recruit many types of RNA to their surfaces. To begin to understand how self-assembled RNA condensates recruit mRNAs, I *in vitro* transcribed a variety of fluorescent mRNAs and observed their localization to homopolymer condensates. All homopolymer droplets, including polyA (Figure 3A), recruit *in vitro* transcribed RNA to their surfaces, though polyC droplets initially recruit RNAs to the interior, with RNAs transiting to the surface over time (Figure S2). Thus, RNAs may be recruited to RNA self-assembly surfaces both from condensate interiors and the external solultion. These data also suggest that the recruitment of mRNAs to the surfaces of biological RNP assemblies may be favorable, stabilizing those systems.

To test whether RNP granules can recruit mRNA to their surfaces, I stressed human U-2 OS cells expressing a stable GFP-G3BP1 fusion protein (to label SGs) with $NaAsO_2$. I then

purified the SGs with successive centrifugations (Khong *et al.*, 2017). Afterwards, I incubated the purified SGs with fluorescent *in vitro* transcribed *luc* RNA (Figure 3B). I observed that *luc* could localize to the surface of SGs (Figure 3C), indicating that a SG can interact with RNA. These data suggest that SGs, and perhaps similar RNP granules, are capable of forming surface interactions with RNA in cells, recruiting and concentrating it.

Many neurodegenerative and muscle wasting diseases, like ALS and myotonic dystrophy, are caused by repeat expansions in particular genes, leading to the production of repeat expansion RNAs (reRNAs) and abnormal protein products (Nelson *et al.*, 2013). These reRNAs readily self-assemble *in vitro* and form gelatinous foci inside cells that may be pathogenic (Jain and Vale, 2017). To test whether reRNA foci could recruit and assemble RNA on their surfaces, I *in vitro* transcribed a fluorescent RNA containing exons 11-15 of *DMPK* followed by ~590 CUG repeats to model the aberrant RNA species present during myotonic dystrophy type 1. I condensed the CUG reRNA in the presence of other fluorescently labeled RNAs and observed that mRNA could be recruited to puncta on the surfaces of CUG reRNA assemblies (Figure 3D), though PTR was internalized (Figure S2). Thus, CUG repeat foci, and perhaps other reRNA foci, are capable of assembling many types of RNA on their surfaces, likely reducing surface free energy and stabilizing the system, while the internalization of PTR is probably attributable to some combination of internalizing interactions with the reRNA and its smaller size.

Altogether, a wide diversity of RNA/RNP assemblies recruit RNA to their surfaces. This suggests that some RNAs may be able to behave similarly in some ways to surfactants, stabilizing interfaces between heterotypic condensates and within multiphase assemblies. To test this, I observed the co-assembly of polyC, polyU, and fluorescent *pgc* mRNA. This led to the formation of polyC/polyU multi-phase assemblies (Figure 3E) with *pgc* RNA localized robustly to the polyC/polyU interface, consistent with its individual localization to both homopolymers (Figure S3).

The examples of RNA homopolymer self-assemblies, SGs, and reRNA foci illustrate that surface recruitment and concentration of RNAs from the solution is a common property of RNA self-assembly and RNP assemblies. These surface assemblies are expected to reduce the free energy of the system, and therefore, could potentially stabilize RNP granules in the cell. In league with this, interfacial RNA can promote the formation of multiphase assemblies, stabilizing them. This could have implications for multiphase RNP compartments like the nucleolus or for the docking of different RNP granules, such as the docking of P bodies and SGs (Kedersha *et al*., 2005).

Surface free energy promotes RNA self-assembly by stabilizing intermolecular interactions

It is known that condensed phases like oil/water emulsions can recruit certain particles to their surfaces and form stable shells (Pickering, 1907; Cakmak and Keating, 2017; Yang *et al*., 2017). This is a fundamental property of condensed matter arising from the free energy of the interface between a condensate and the solvent, which can be reduced by the adsorption of particles onto the surface. These particles can interact to form stable, solid-like puncta or shells and thereby stabilize the condensate system.

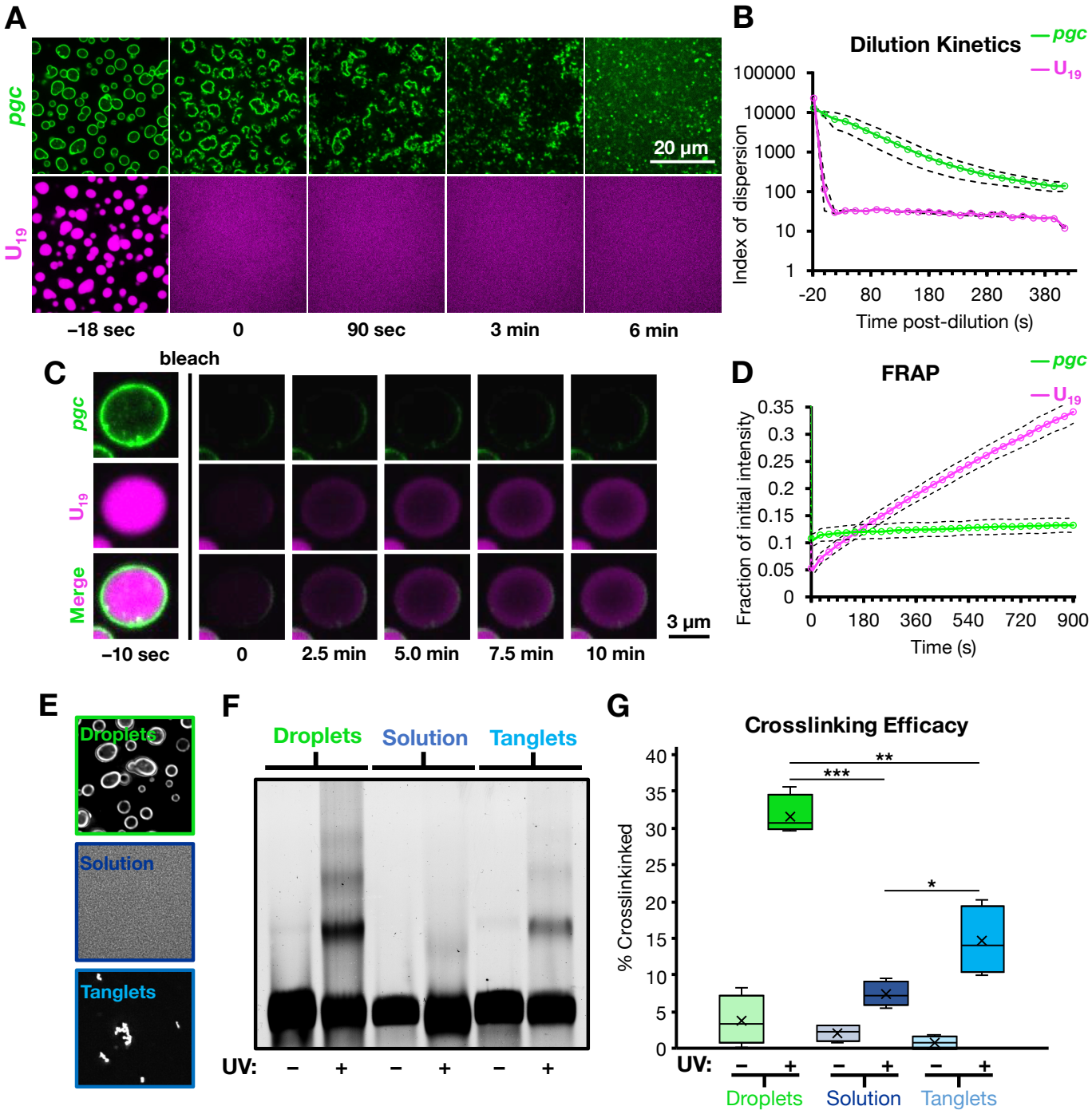

Figure 4. RNA condensate surfaces stabilize intermolecular RNA-RNA interactions and promote stable self-assembly by reducing surface free energy. **(A)** PolyA/*pgc* co-assemblies were diluted 1:10 into TE buffer and imaged over time, showing a quick loss of droplets but a persistent *pgc* shell. **(B)** Quantification of (A), illustrating that *pgc* assemblies persist for several minutes post-dilution. Dashed lines represent 95% confidence intervals. **(C)** Representative images of *pgc* and U_{19} recovery in a polyA/*pgc* co-assembly following photobleaching. Scale bar is 3 µm. **(D)** Quantification of (C), showing that while U_{19} slowly recovers, *pgc* does not recover and is almost fully immobile. Dashed lines represent ±1 standard deviation of the mean. **(E)** The three crosslinking conditions. "Droplets" refers to polyA/*pgc* co-assemblies, "Solution" to the same amount of *pgc* and polyA together in solution in TE, and "Tanglets" refers to the small, gel-like self-assemblies of *pgc* when it is condensed alone (without polyA) at the same concentration. **(F)** Representative fluorescence denaturing gel of crosslinking products. Higher-weight bands correspond to crosslinked *pgc* multimers. **(G)** Quantification of (F). While solution conditions yield minimal crosslinking and tanglets show increased *trans pgc-pgc* interactions, droplets have double the crosslinking as tanglets, implying that recruitment to droplets enhances *pgc-pgc* interactions. *$p<0.05$, **$p<0.01$, ***$p<10^{-4}$.

To test whether the RNA recruited to RNA condensate surfaces is similarly more stable than the underlying condensate, I prepared polyA/*pgc* co-assemblies (visualizing polyA with fluorescent U_{19}) and diluted them 1:10 with TE buffer (Figure 4A). Following dilution, the polyA droplets dissolved within seconds, whereas the *pgc* shell persisted for many minutes (Figure 4B). Second, I performed FRAP on the co-assemblies, with the polyA labeled by fluorescent U_{19} (Figure 4C). While the U_{19} signal was recovering, the *pgc* showed virtually no recovery (Figure 4D), showing the *pgc* shell to be stable.

To understand the physical basis behind why RNAs on condensate surfaces form such stable assemblies, I incubated fluorescent *pgc* RNA in three separate conditions (Figure 4E) in the presence of 4'-aminomethyltrioxsalen, a psoralen derivative that crosslinks nucleic acid duplexes in UV light (Frederikson and Hearst, 1979). I then crosslinked the RNA, recovered it in LiCl, and analyzed it on a denaturing gel by visualizing the *pgc* fluorescence (Figure 4F). While *pgc* in solution demonstrated minimal crosslinking, the *pgc* in tanglets showed a higher fraction crosslinked and the presence of higher-weight multimers (Figure 4G). By comparison, *pgc* recruited to the surfaces of droplets displayed an even greater degree of crosslinking (~2×) and multimerization than that in the tanglets, implying that intermolecular RNA-RNA interactions are stabilized by droplet surfaces. This is consistent with surface free energy driving the adsorption, concentration, and interaction of RNAs on condensate surfaces.

In summary, RNA self-assemblies, and likely RNP granules, recruit a variety of RNAs to their surfaces by reducing surface free energy. In turn, recruited RNAs are concentrated, and their intermolecular interactions are stabilized, leading to the formation of a hyperstable surface shell. Thus, RNP granule surfaces are expected to be capable of promoting the intermolecular interactions of localized RNAs.

<u>eIF4A helicase activity modulates RNA recruitment to SGs in human cells</u>

RNA self-assembly is a thermodynamically favorable process, exemplified in part by the modest concentrations required for self-assembly (Van Treeck *et al*., 2018). Moreover, the presence of an RNA or RNP condensate further lowers the energy of forming new intermolecular RNA-RNA interactions by providing a surface off of which other RNA-RNA interactions (Figure 3, Figure 4) and even other RNA condensates (Figure 2) can nucleate. This implies that cells have one or more mechanisms to limit or otherwise modulate RNA self-assembly, and prevent the uncontrolled aggregation of RNA.

RNA helicases could fill this role, and by far, the most abundant helicase in the cell is the essential translation initiation factor eIF4A (Itzhak *et al*., 2016). Since it is present in SGs as well (Jain *et al*., 2016), it is a natural candidate for modulating RNA condensation onto SGs.

To assess if eIF4A influences the recruitment of RNAs to SGs, I stressed human U-2 OS cells with $NaAsO_2$, then treated them with control solution, the eIF4A helicase inhibitor hippuristanol (Bordeleau *et al*., 2006), or inhibitors of glycolysis and oxidative phosphorylation, depleting ATP (presumably inhibiting all helicases). Afterwards, I fixed the cells, immunostained for the SG marker protein PABPC1, and performed single molecule fluorescence *in situ* hybridization (smFISH) for *TFRC* or *POLR2A* mRNAs.

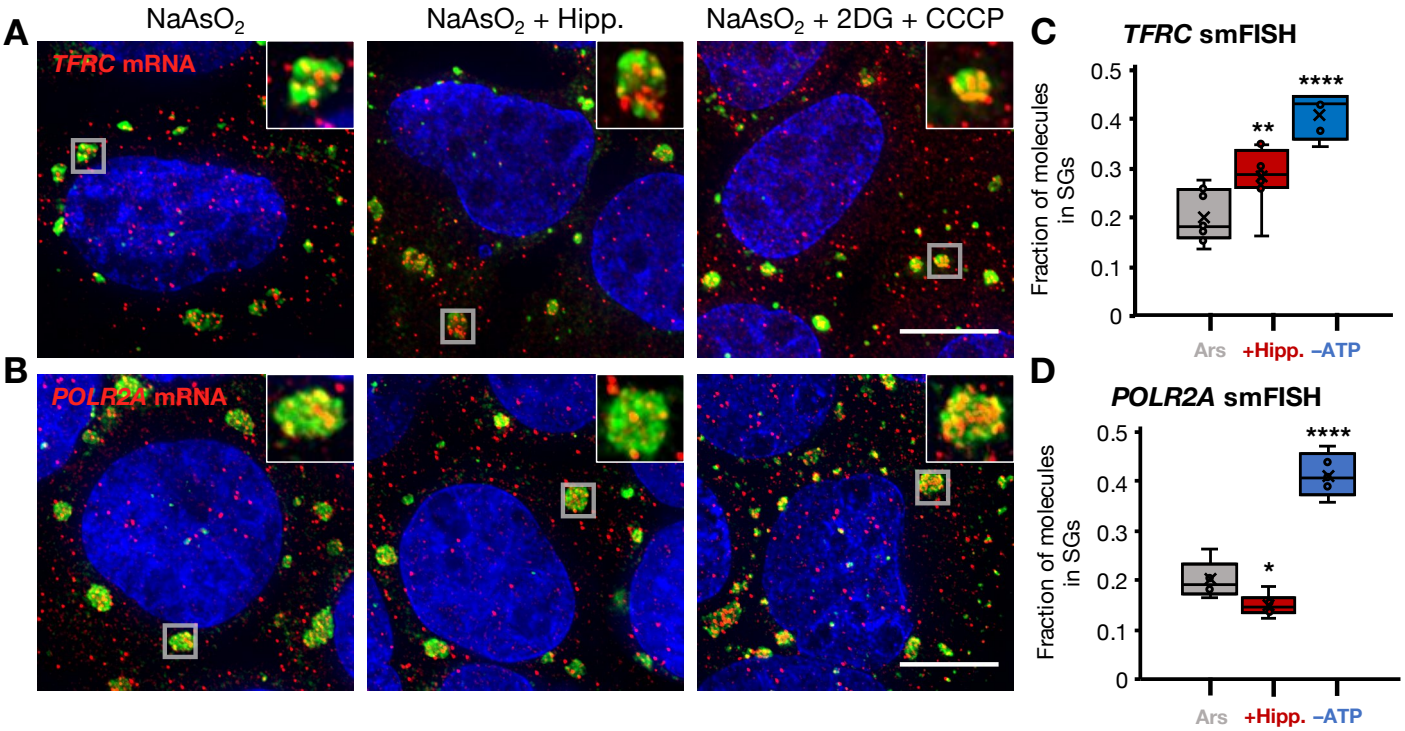

Figure 5. The RNA helicase eIF4A and potentially others modulate the recruitment of RNAs to SGs. Human U-2 OS cells were stressed 1 h with 500 μM $NaAsO_2$, and then afterwards treated for 30 min with 300 nM hippuristanol, which inhibits the eIF4A helicase, or 200 mM 2DG and 100 μM CCCP to deplete ATP. Cells were then fixed and stained for PABPC1, a SG marker, and smFISH was performed. **(A)** Representative images of cells in each condition following fixation, staining, and hybridization with smFISH probes against *TFRC* mRNA. Insets show single granules. **(B)** Quantification of the fraction of *TFRC* molecules in SGs reveals that helicase inhibition leads to a greater accumulation of transcripts, and ATP depletion leads to an enhanced effect. **(C)** Representative images of cells following hybridization with smFISH probes against *POLR2A* mRNA. **(D)** Quantification of (C), showing a modest decrease in RNA accumulation in SGs following hippuristanol, but — similarly to *TFRC* — approximately double the mRNAs accumulate in SGs following ATP depletion. **(A, C)** Scale bars are 20 μM and gray boxes denote the inset granules. **(B, D)** $^{*}p<0.05$, $^{**}p<0.01$, $^{****}p<10^{-4}$.

An important result was that hippuristanol treatment following arsenite led to a significant increase in the fraction of *TFRC* molecules in SGs compared to the control (Figure 5A-B). This implies that eIF4A helicase activity can limit the recruitment of *TFRC* to SGs. Moreover, ATP depletion yielded a larger increase in *TFRC* mRNA enrichment. This is consistent with additional ATP-dependent SG remodeling factors, presumably including other RNA helicases, limiting *TFRC* mRNA localization to SGs.

Interestingly, I observed different results with *POLR2A* mRNA, whose partitioning was barely affected by hippuristanol, but was clearly increased by ATP depletion (Figure 5C-D). This suggests that individual mRNPs will have different interactions with SGs and will thereby be differentially sensitive to specific SG remodeling factors (see discussion). These data are also consistent with specific RNA helicases regulating localization of RNAs to SGs, including a role for eIF4A in limiting the recruitment of certain RNAs. The smFISH data therefore helps define a new function for eIF4A in modulating RNA assembly in the cell.

Discussion

My data illustrate many principles and properties of RNA self-assembly. First, and consistent with other studies (Vieregg *et al*., 2018; Van Treeck *et al*., 2018), the strength of intermolecular interactions between RNAs influences the material properties and dynamics of RNA self-assemblies. For example, Watson-Crick interactions can lead to robust, homogeneous partitioning into condensates (Figure 1, Figure S1), low exchange rates (Figure 1C), and the formation of more stable assemblies (Figure 2A). By contrast, noncanonical interactions can produce lower, but far more dynamic partitioning, or stable surface assembly, and can drive homotypic clustering and less viscous assemblies (Van Treeck *et al*., 2018). In cells, weak RNA-RNA interactions could potentially facilitate the formation of dynamic granules, or a labile fraction, with rapidly exchanging pools of RNA. This could be important if RNAs only need to be in granules transiently—for instance, to be spliced in a nuclear speckle. By contrast, strong intermolecular RNA-RNA interactions could promote the formation of more constitutive assemblies with immobile RNA. One possible example could be nuclear paraspeckles, where specific interactions between *NEAT1* domains are important for paraspeckle formation, organization, and integrity (Lin *et al*., 2018).

Another prediction from this particular property of RNA self-assembly is that perturbations that stabilize RNA-RNA interactions, such as elevated intracellular salt concentrations, reduced temperature, ablated helicase activity, or even other RNP granules (Figures 3 and 4), ought to increase the recruitment of RNAs into or onto RNP granules. This would also potentially reduce the RNA dynamics of these assemblies. Consistent with these ideas, sorbitol stress, which increases intracellular salt concentrations, can induce SGs even in the absence of the typically-necessary protein G3BP (Kedersha *et al*., 2016), perhaps overcoming the lost protein-protein interactions with strengthened RNA-RNA interactions. Moreover, other work from our lab has shown that inhibition of the eIF4A helicase with hippuristanol leads to increased partitioning of polyadenylated RNA in SGs, consistent with eIF4A limiting the RNA-RNA interactions that drive mRNA condensation.

A second property of RNA self-assembly is that weak interactions can drive homotypic clustering, and these compartments can arrange into organized networks (Figure 2) by minimizing surface free energy. Thus, RNA is capable of spontaneously forming self-propagating patterns when assembled. Within a cellular context, this principle may have applications to the *Drosophila* germ plasm, which contains homotypic clusters of maternal mRNAs localized into specific homotypic clusters (Trcek *et al*., 2015). It is possible that RNA homotypic clustering and self-patterning promotes this organization of maternal mRNAs within the germ plasm. It may also be relevant to the spatial association between P bodies and SGs (Kedersha *et al*., 2005) and between splicing speckles and nuclear paraspeckles (Fox *et al.*, 2002).

A third property of RNA self-assembly is that the surfaces of RNA and RNP condensates stabilize intermolecular RNA-RNA interactions by reducing surface free energy, producing stable RNA aggregates (Figure 4, Figure 6). This surface assembly process, along with other types of RNA self-assembly, is thermodynamically favorable and therefore could be expected to create problems for the cell if it continued unchecked (Figure 6B), namely excessive RNA aggregation.

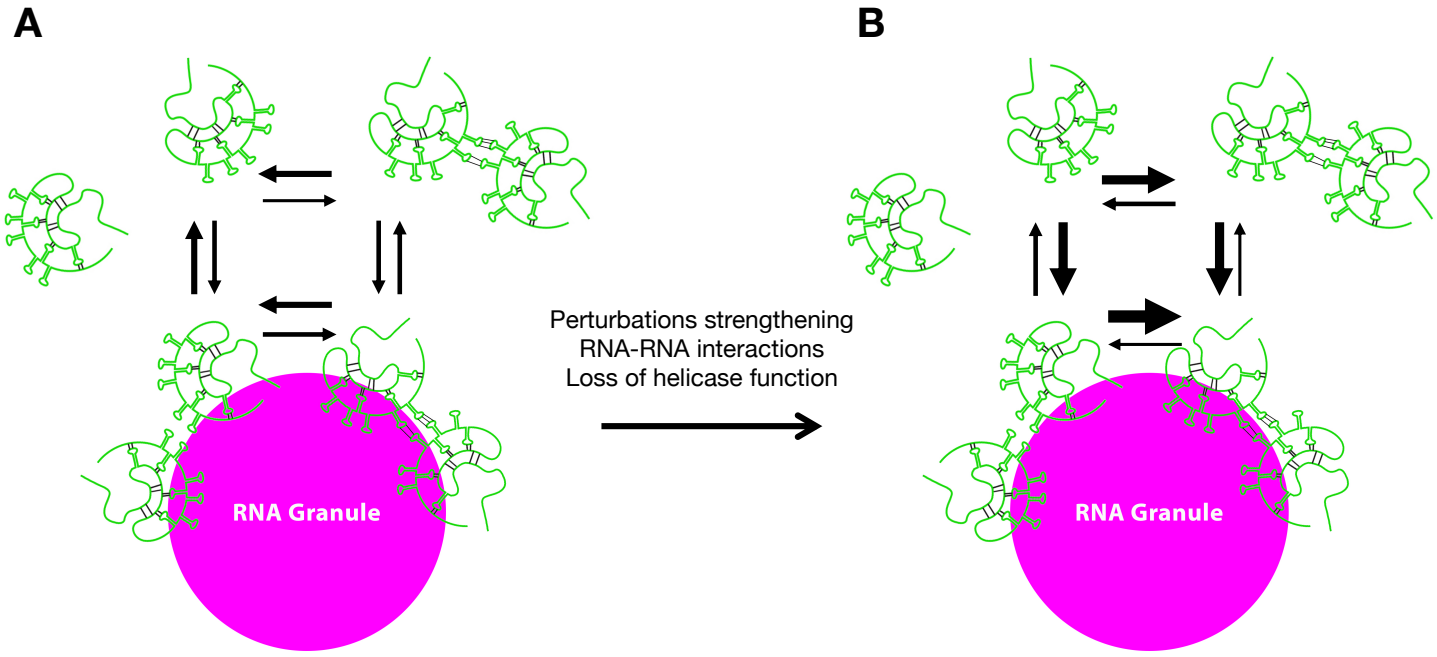

Figure 6. (A) In typical conditions, adsorption onto RNP granules is expected to be thermally favorable, but combated by ATP-dependent machinery, in particular RNA helicases. This allows the cell to escape the energy well and to maintain pools of free RNA. **(B)** In contrast, perturbations promoting the interaction of RNAs, such as the failure of that ATP-dependent machinery, lead to a shift in the net equilibrium from free RNA to interacting RNA, promoting RNA self-assembly.

RNA helicases may modulate the formation, content, and dynamics of RNP granules in the cell (Figure 6). Correspondingly, inhibition of the eIF4A helicase with hippuristanol following arsenite stress led to an increased SG enrichment of *TFRC*, mRNA in cells as assessed by smFISH (Figure 5). Furthermore, ATP depletion induces an even more robust partitioning of both *TFRC* and *POLR2A* mRNAs, consistent with other ATP-dependent SG remodeling factors, probably including RNA helicases, limiting RNA condensation in the cell. In contrast to *TFRC*, hippuristanol treatment does not substantially affect the partitioning of *POLR2A* mRNA into SGs. There are multiple possible reasons underlying this discrepancy. First, different RNAs may have different modes of recruitment to SGs: some mRNAs (perhaps including *TFRC*) may partition to SGs through promiscuous intermolecular RNA-RNA interactions, whereas others (perhaps including *POLR2A*) may partition to granules due to multivalent protein-protein interactions between RNA binding proteins. In the former case, the mRNA partitioning would be expected to be sensitive to eIF4A, whereas it would not be in the latter. Second, different RNA helicases could have preferential or specific mRNA substrates, leading to mRNA-specific effects. For example, in translating conditions, eIF4A activity is observed to preferentially affect mRNAs with long, structured 5' UTRs (Sen *et al*., 2016), though it is not clear if this preference would be maintained during stress. Thus, eIF4A may limit the condensation of a wide, but not comprehensive, variety of RNAs in the cell.

There is some evidence of helicases in other RNP granules behaving similarly to eIF4A. Notably, siRNA knockdown of the speckle RNA helicase UAP56/DDX39b leads to increased polyA$^+$ RNA accumulation in speckles (Dias *et al*., 2010), analogous to eIF4A and SGs. Similarly, the nuclear helicase DDX21 is localized in rings along the peripheries of nucleoli (Calo *et al*., 2015) and RNA PolI complexes (Xing *et al*, 2017). These lines of evidence argue

that RNA helicases may in fact limit the condensation of RNA, or specific types of RNA, in other RNP granules.

Conditions of cold or high salt should stabilize RNA-RNA interactions, promoting self-assembly (Figure 6). Intriguingly, across all domains of life, cold shock proteins are enriched in RNA helicases and monomeric RNA binding proteins that dissolve RNA-RNA interactions (Rennella *et al*., 2017; Phadtare and Severinov, 2018). RNA helicases are also upregulated in response to high salt stress and confer stress tolerance in *Arabidopsis* and other plants (Zhu *et al*., 2015; Nguyen *et al*., 2018; Nawaz and Kang, 2019). Together, these findings hint at a broader role for RNA helicases in maintaining and modulating the RNA condensation state of the cell.

These results raise several questions for continuing and future research. First, do RNA helicases modulate the condensation and dynamics of other RNP granules? Given the presence of high concentrations of RNA (Van Treeck and Parker, 2018) and the presence of RNA helicases in virtually all RNP granules, I hypothesize that the balance between spontaneous RNA self-assembly and ATP-dependent modulation is important for many RNP granule types, and this could be revealed with experiments similar to those done with eIF4A. Second, do stressors like cold shock or high salt promote granulation by stabilizing intermolecular RNA-RNA interactions? If so, then RNA granulation and partitioning conceivably could be modulated by altering salt concentrations or temperature, and perhaps granules such conditions could be removed by expressing helicases, with potential implications for salt stress response. Third, what intermolecular interactions are important for RNA self-assembly or homotypic clustering? Are there specific H-bonding regimes more prevalent in labile assemblies than in stable ones, and are these interactions biologically relevant? Finally, what are the functional consequences of perturbations in the RNA self-assembly state of the cell? For instance, over-assembled RNA, like in a repeat expansion disorder, may itself be pathogenic (Jain and Vale, 2017).

Altogether, I have developed a number of principles and properties for RNA self-assemblies that all may have cellular implications. I have also presented evidence consistent with the model that the processes of RNA self-assembly and condensation onto RNP granules in the cell are modulated by RNA helicases, solving the problem of the favorable energetics of assembly. The broad implication of this work is that the properties of RNA self-assembly and its modulation by helicases are important for RNP granule status, and may therefore be influential in various stages of RNA metabolism and in granule-associated diseases like many kinds of neurodegeneration.

Acknowledgements

First, I thank the entire Parker lab and Olke Uhlenbeck for providing a tremendously enriching environment to learn and grow as a scientist the past couple years, in addition to great questions, ideas, and discussions. In particular, I would especially like to express my gratitude to Briana Van Treeck for helping me get this project going, for her excellent ideas when things weren't working, and for always being willing to read something I found or comment on a result. I would also like to thank Carolyn Decker for providing me with DeltaVision training and helping me learn the ropes in the Parker lab my first few months. I gratefully acknowledge Matt Disney (Scripps) for providing the reRNA transcription plasmids, the Drosophila Genomics Research Center (Bloomington, IN) for providing fly RNA plasmids, and John Rinn (CU Boulder) for

providing the *Firre* transcription plasmid. I also acknowledge Joe Dravagon and the BioFrontiers Institute Advanced Light Microscopy Core Facility, where much of the data for this work was collected and analyzed, as well as Theresa Nahreini and the BioFrontiers Institute Cell Culture Facility. I especially thank Roy for the tremendous time, energy, and mentorship he provided. Finally, I want to thank Tom Cech and Brian DeDecker for taking the time to be on my committee.

This work was funded in part by a Undergraduate Research Opportunity Program grant from the CU College of Arts and Sciences and by the Howard Hughes Medical Institute (to R.P.).

Methods

Homopolymer condensation

Homopolymer RNAs were purchased as salts from Amersham Pharmacia Biotech, Inc. (polyA, polyC, and polyU) and Sigma-Aldrich (polyU) and made into 25 mg/mL stock solutions in TE (10 mM tris, 1 mM EDTA, pH 8.0) or RNase-free water (Invitrogen), then kept at –80°C. Working 5 mg/mL stock solutions were prepared by diluting into RNase-free water. These working stocks were stored at –80°C or –20°C. The fluorescently-labeled oligonucleotides were purchased from IDT and resuspended, from which 2 µM stock solutions were made and stored at –80°C. An initial aliquot of the fluorescently-labeled PTR (*p*olypyrimidine *t*ract *R*NA; $[UCUCUAAAAA]_5$) was generously provided by the Rosen lab at UT Southwestern. More was purchased from IDT and was stored at –80°C as a 2 µM stock solution.

To form homopolymer condensates for the short RNA localization experiments, homopolymer RNA was mixed with small RNA probes, heated at 90°C for 1.5 min to denature pre-existing structures, cooled on ice 1 min, quickly vortexed and spun, then mixed with 750 mM NaCl and 10% w/v PEG 3350 (Sigma) at a final homopolymer concentration of 0.5 mg/ml and a final RNA probe concentration of 200 nM. The mixtures were incubated at room temperature as described previously (Van Treeck *et al*. 2018).

To localize *in vitro* transcribed RNAs, homopolymer RNA was heated and cooled with the transcribed RNA in the same manner as above, but instead mixed with 150 mM NaOAc, 600 mM NaCl, 1 mM $MgCl_2$, and 10% w/v PEG 3350 (all in RNase-free water) to a final homopolymer concentration of 0.4 mg/ml and a final mRNA/lncRNA concentration of 10 µg/ml, yielding an approximate pH of 7 as assessed by litmus paper.

Dispersion indices

The index of dispersion (DI) is a statistical measure of inhomogeneity in a population and is defined to be

$$\mathrm{DI} = \frac{\sigma^2}{\mu},$$

where σ^2 is the variance of the population distribution (with σ being the population standard deviation) and μ is the mean value. For example, particles in ideal solution exhibit a dispersion index of 1, as they are Poisson distributed, and substantially higher values indicate particle-

particle interactions in that context. Here, dispersion indices were used to quantify inhomogeneity in fluorescence signal and infer the relative extent to which an RNA is assembled, similarly to Jain and Vale (2017).

Indices of dispersion were computed from deconvoluted images by measuring the mean fluorescence intensity and standard deviation for maximum projections of 1 μm Z-stacks. An index was computed for each image using ImageJ, and the displayed index was taken to be the average of the indices for all the separate images. The standard deviations for the distribution of index values for a given set of conditions were used to calculate 95% confidence intervals.

In vitro transcription of RNAs

Drosophila nos, *pgc*, *ccr4*, and *cycB* T7 transcription plasmids were procured from the Drosophila Genomics Research Center (DGRC; Bloomington, IN). The m*Firre* 3.1 T7 transcription plasmid was generously provided by the Rinn lab at CU Boulder. The reRNA constructs were generously provided by the Disney lab (Scripps Research Institute). Plasmids were linearized via restriction digestion with BamHI-HF for the fly RNAs, Afe1 for luciferase, and Kpn1-HF for *Firre* (enzymes from New England Biolabs [NEB]). The CUG repeat construct was linearized with HindIII-HF (NEB). Restriction digestion reactions were performed according to the manufacturers' recommendations. Following linearization, plasmid DNA was recovered with ethanol precipitation followed by resuspension in TE buffer.

In vitro transcription of fluorescent RNAs was performed using the T7 MEGAscript kit (Ambion) according to the manufacturer's recommendations with the following modification: Addition of unlabeled UTP was reduced by 25% and an equal amount of fluorescently labeled UTP (fluorescein-12-UTP or cyanine-5-UTP, Enzo Life Sciences) was added in to the reaction mixture. Following transcription, DNA was removed by treating with TURBO DNase (Ambion) according to the manufacturer's recommendations. RNA was recovered by sequential acid phenol/chloroform and chloroform extraction, followed by precipitation in isopropanol and NH_4OAc. RNA recovery was quantified with UV-Vis at 260 nm using a Nanodrop 2000 device (Thermo). Proper RNA sizes were validated through either denaturing gel electrophoresis or Agilent TapeStation RNA ScreenTape analysis (performed by the BioFrontiers Next-Generation Sequencing Core Facility). Recovered RNA was resuspended in RNase-free water (Invitrogen) and stored at –80°C. Working 100 μg/ml stocks were created as needed by diluting appropriately into RNase-free water, and were kept at –80°C.

RNA condensation-crosslinking assays

To observe RNA-condensate-associated RNA-RNA interactions, 4'-aminomethyltrioxsalen (AMT) crosslinking was performed (Frederikson and Hearst, 1979). AMT was procured from Santa Cruz Biotechnology and solubilized to a final concentration of 1 mg/ml. AMT stocks were stored at –20°C. Since AMT crosslinks pyrimidine residues, condensation-crosslinking experiments were performed using polyA condensates.

In condensation-crosslinking experiments, RNA was demixed in the appropriate buffer for the experiment, but with the addition of 100 μg/ml AMT. Following incubation, RNA was

crosslinked by irradiating 15 min with 366 nm UV light. Afterwards, samples were diluted 1:1.7 in TE and RNA was recovered by precipitation in 2 M LiCl. If RNA sample concentrations were low (e.g., tanglet conditions), 0.4-0.5 mg/ml polyA homopolymer RNA was added post-crosslinking and pre-precipitation as a carrier in order to promote efficient recovery.

Denaturing gel electrophoresis

Denaturing gel electrophoresis was performed to analyze fluorescent and crosslinked RNAs. RNA samples were mixed with either 6× formaldehyde loading dye (Ambion) or 2× formamide loading dye (95% deionized formamide, 0.025% w/v bromophenol blue, 5 mM EDTA) and denatured by incubation at 70°C for 15 min, followed by incubation on ice for 3 min. Samples were run in freshly-prepared 1% agarose, 1% formaldehyde denaturing gels in fresh 1× MOPS buffer (20 mM MOPS, 5 mM NaOAc, 1 mM EDTA, pH 7) at 4-10 V/cm for 2.5-4 hours.

Denaturing gels were imaged using a Typhoon FLA 9500 imaging system (GE) set to visualize the appropriate fluorescence signal from fluorescently-labeled RNAs. Crosslinking efficacies were quantified in ImageJ by measuring the integrated intensities of the monomer bands and higher-weight bands, subtracting the average of 10-15 background measurements, and dividing the sum of the corrected higher-weight integrated intensities by the sum of all band integrated intensities. In symbols:

$$\mathrm{CE} = \frac{\sum_{n=2}^{N} I_n}{\sum_{n=1}^{N} I_n} \times 100\%\,,$$

where I_n is the (background-corrected) integrated intensity of the band corresponding to the RNA n-mer, N is the highest order band observed in a given sample, and CE is the crosslinking efficacy.

Assembly dilution assays

To test the stability of RNA assemblies under dilution, *pgc*-decorated polyA droplets were prepared as above and incubated 2 hours. Thereafter, they were subjected to spinning disk confocal timelapse microscopy. Every 18 sec, an image was taken in each channel in a 4x4 grid of adjacent frames using the Nikon Elements software “Large Image” feature. These images were automatically stitched together, and each replicate was quantitated by dispersion index.

Dilutions were performed while imaging was ongoing. In between imaging timepoints, TE buffer was quickly added dropwise (so as to only minimally disturb assemblies) to a tenfold final dilution. The very next imaging timepoint was taken to be t=0 for quantitative analysis.

Cell culture

Human osteosarcoma U-2 OS parental and stable GFP-G3BP1 cells were maintained in DMEM with high glucose, 10% fetal bovine serum, and 1% penicillin/streptomycin at 37°C and 5% CO_2.

SG isolation

To test the ability of SGs to recruit *in vitro* transcribed RNAs, SGs were purified as follows: First, GFP-G3BP1 U-2 OS cells were seeded at ~40% confluency and then grown to ~80% confluency, after which the media was replaced and the cells were stressed with 500 µM $NaAsO_2$ for 60 min. Afterwards, the cells were washed, pelleted, and flash-frozen in liquid N_2, then stored at –80°C for up to a week. SGs were isolated as in Khong *et al*. (2017) to produce SG-enriched fraction. No affinity purification was performed. Other cellular debris was removed from the SG-enriched supernatant through both vigorous pipetting and by passing the supernatant through a 25G 5/8 needle, accompanied by quick spins.

Repeat expansion RNA condensation and surface assembly

To assess the ability of reRNA foci to sequester RNAs, foci were prepared by condensing 200 µg/ml of fluorescein-labeled $(CUG)_{590}$ as in Jain and Vale (2017) in the presence or absence of 10 µg/ml Cy5-labeled *in vitro* transcribed RNAs or 200 nM PTR-Cy3. Briefly, RNAs were mixed together in a buffer of 10 mM $MgCl_2$, 10 mM Tris HCl pH 6.8, and 25 mM NaCl, and subsequently denatured for 3 min at 95°C then cooled at ~4°C/min to 37°C in a thermocycler. Afterwards, condensates were immediately imaged.

Fluorescence recovery after photobleaching (FRAP)

Droplets were prepared as described above, and imaged with a Nikon A1R laser scanning confocal. Three images were taken followed by photobleaching droplets and imaging over the course of recovery.

To analyze recovery, the mean intensity of each bleached region was quantified in ImageJ, and recovery intensities were normalized to the mean of three pre-bleach measurements. Mobile fractions ϕ_M were computed by subtracting the minimum normalized mean intensity I_0 from the normalized endpoint intensity I_F: $\phi_M = I_F - I_0$. To calculate $t_{1/2}$ values, FRAP data was fit in MATLAB to the equation $\phi_R(t) = \phi_M \cdot (1 - e^{-\tau t} + c)$, where $\phi_R(t)$ is the fraction recovered at time t and c is a constant term to account for incomplete photobleaching. The fit yielded values for τ that were used to calculate $t_{1/2}$ according to $t_{1/2} = \ln(1/2)/-\tau$.

Fluorescence microscopy

Most experiments were imaged using a DeltaVision widefield microscope equipped with a standard 100× oil objective. Following imaging, images were deconvolved with the provided software. Some homopolymer surface assembly experiments and the dilution timelapses were imaged using a Nikon Ti Eclipse spinning disk confocal microscope equipped with a 100× oil objective. FRAP images were acquired using a Nikon A1R laser scanning confocal equipped with a 100× oil objective.

Immunofluorescence and single molecule FISH

For the IF/smFISH experiments, U-2 OS cells were stressed for 1 hour with 500 µM $NaAsO_2$ (Sigma), followed by treatment for 30 min with either buffer, 300 nM hippuristanol

(generously provided by the Pelletier lab at McGill University, Toronto), or 200 mM 2-deoxy-D-glucose (2DG, Sigma) and 100 μM carbonyl cyanide *m*-chlorophenol hydrazine (CCCP, Sigma). Afterwards, cells were washed, fixed in 4% paraformaldehyde for ten minutes at room temperature, and permeabilized with 0.1% Triton-X 100 (Sigma) for five minutes at room temperature. Antibody staining with rabbit polyclonal PABPC1 antibody (Abcam) and smFISH probe hybridization for *TFRC* or *POLR2A* (Stellaris) was performed as in Khong *et al*., 2017. Images were analyzed as whole Z-stacks using Imaris software (Bitplane).

References

P. Anderson, N. Kedersha. RNA granules. *J. Cell Bio.* **172**, 803-808 (2006).

W. M. Aumiller, Jr., C. D. Keating. Phosphorylation-mediated RNA/peptide complex coacervation as a model for intracellular liquid organelles. *Nat. Chem.* **8**, 129-137 (2016).

W. M. Aumiller, Jr., F. Pir Cakmak, B. W. Davis, C. D. Keating. RNA-Based Coacervates as a Model for Membraneless Organelles: Formation, Properties, and Interfacial Liposome Assembly. *Langmuir* **32**, 10042-10053 (2016)

S. F. Banani, H. O. Lee, A. A. Hyman, M. K. Rosen. Biomolecular condensates: organizers of cellular biochemistry. *Nat. Rev. Mol. Cell Biol.* **18**, 285-298 (2017).

P. R. Banerjee, A. N. Millin, M. M. Moosa, P. L. Onuchic, A. A. Deniz. Reentrant Phase Transition Drives Dynamics Substructure Formation in Ribonucleoprotein Droplets. *Angew. Chem. Int. Ed. Engl.* **56**, 11354-11359 (2017).

S. Boeynaems, S. Alberti, N. L. Fawzi, T. Mittag, M. Polymenidou, F. Rousseau, J. Schymkowitz, J. Shorter, B. Wolozin, L. Van Den Bosch, P. Tompa, M. Fuxreiter. Protein Phase Separation: A New Phase in Cell Biology. *Trends Cell Biol.* **28**, 420-435 (2018).

M. E. Bordeleau, A. Mori, M. Oberer, L. Lindquist, L. S. Chard, T. Higa, G. J. Belsham, G. Wagner, J. Tanaka, J. Pelletier. Functional characterization of IRESes by an inhibitor of the RNA helicase eIF4A. *Nat. Chem. Biol.* **2**, 213-220 (2006).

O. Bounedjah, B. Desforges, T. D. Wu, C. Pioche-Durieu, S. Marco, L. Hamon, P. A. Curmi, J. L. Guerquin-Kern, O. Piétrement, D. Pastré. Free RNA in excess upon polysome dissociation is a scaffold for protein multimerization to form stress granules. *Nucleic Acids Res.* **43**, 8678-8691 (2014).

E. Calo, R. A. Flynn, L. Martin, R. C. Spitale, H. Y. Chang, J. Wysocka. Nuclear helicase DDX21 coordinates transcription and ribosomal RNA processing. *Nature* **518**, 249-253 (2015).

K. Chalupnikova, S. Lattmann, N. Selak, F. Iwamoto, Y. Fujiki, Y. Nagamine. Recruitment of the RNA helicase RHAU to stress granules via a unique RNA-binding domain. *J. Biol. Chem.* **283**, 35186-98 (2008).

K. M. Creamer, J. B. Lawrence. *XIST* RNA: a window into the broader role of RNA in nuclear chromosome architecture. *Phil. Trans. R. Soc. Lond. B Biol. Sci.* **372**, doi: 10.1098/rstb.2016.0360 (2017).

A. P. Dias, K. Dufu, H. Lei, R. Reed. A role for TREX components in the release of spliced mRNA from nuclear speckles. *Nat. Commun.* **2010**, 1:97. doi: 10.1038/ncomms1103.

A. H. Fox, A. I. Lamond. Paraspeckles. *Cold Spring Harbor Perspect. Biol.* **2**, a000687. doi: 10.1101/cshperspect.a000687 (2010).

A. H. Fox, Y. W. Lam, A. K. Leung, C. E. Lyon, J. Andersen, M. Mann, A. I. Lamond. Paraspeckles: a novel nuclear domain. *Curr. Biol.* **8**, 13-25 (2002).

S. Frederikson, J. E. Hearst. Binding of 4'-aminomethyl 4,5',8-trimethyl psoralen to DNA, RNA, and protein in HeLa cells and *Drosophila* cells. *Biochim. Biophys. Acta* **563**, 343-355 (1979).

V. L. Golo, E. I. Kats, Y. S. Volkov, V. I. Salyanov, Y. M. Yevdokimov. Novel Cholesteric Phase in Dispersions of Nucleic Acid due to Polymeric Chelate Bridges. *J. Biol. Phys.* **27**, 81-93 (2001).

A. Hillicker, Z. Gao, E. Jankowsky, R. Parker. The DEAD-box protein Ded1 modulates translation by the formation and resolution of an eIF4F-mRNA complex. *Mol. Cell* **43**, 962-72 (2011).

A. Hubstenberger, M. Courel, M. Bénard, S. Soquere, M. Ernoult-Lange, *et al*. P body purification reveals the condensation of repressed mRNA regulons. *Mol. Cell* **68**, 144-57 (2017).

D. N. Itzhak, S. Tyanova, J. Cox, G. H. H. Borner. Global, quantitative and dynamic of protein subcellular localization. *eLife* **5**, e16950 (2016).

A. Jain, R. D. Vale. RNA phase transitions in repeat expansion disorders. *Nature* **546**, 243-247 (2017).

S. Jain, J. R. Wheeler, R. W. Walters, A. Agrawal, A. Barsic, R. Parker. ATPase-modulated stress granules contain a diverse proteome and substructure. *Cell* **164**, 487-489 (2016).

I. Jarmoskaite, R. Russell. RNA helicase proteins as chaperones and remodelers. *Ann. Rev. Biochem.* **83**, 697-725 (2014).

N. Kedersha, M. D. Panas, C. A. Achorn, S. Lyons, S. Tisdale, T. Hickman, M. Thomas, J. Lieberman, G. M. McInnery, P. Ivanov, P. Anderson. G3BP-Caprin1-USP10 complexes mediate stress granule condensation and associate with 40S subunits. *J. Cell Biol.* **212**, 845-60 (2016).

N. Kedersha, G. Stoecklin, M. Ayodele, P. Yacono, J. Lykke-Andersen, M. J. Fritzler, D. Scheuner, R. J. Kaufman, D. E. Golan, P. Anderson. Stress granules and processing bodies are dynamically linked sites of mRNP remodeling. *J. Cell Biol.* **169**, 871-84 (2005).

A. Khong, S. Jain, T. Matheny, J. R. Wheeler, R. Parker. Isolation of mammalian stress granule cores for RNA-seq analysis. *Methods* **137**, 49-54 (2017).

A. Khong, T. Matheny, S. Jain, S. F. Mitchell, J. R. Wheeler, R. Parker. The Stress Granule Transcriptome Reveals Principles of mRNA Accumulation in Stress Granules. *Mol. Cell* **68**, 808-820 (2017).

E. M. Langdon, Y. Qiu, A. Ghanbari Niaki, G. A. McLaughlin, C. A. Weidmann, T. M. Gerbich, J. A. Smith, J. M. Crutchley, C. M. Termini, K. M. Weeks, S. Myong, A. S. Gladfelter. mRNA structure determines specificity of a polyQ phase transition. *Science* **360**, 922-927 (2018).

Y. Lin, B. F. Schmidt, M. P. Bruchez, C. J. McManus. Structural analyses of NEAT1 lncRNAs suggest long-range interactions that may contribute to paraspeckle architecture. *Nucleic Acids Res.* **46**, 3742-3752 (2018).

P. Linder, F. V. Fuller-Pace. Looking back on the birth of DEAD-box RNA helicases. *Biochim. Biophys. Acta* **1829**, 750-5 (2013).

C. F. Mugler, M. Hondele, S. Heinrich, R. Sachdev, P. Vallotton, A. Y. Koek, L. Y. Chan, K. Weiss. ATPase activity of the DEAD-box protein Dhh1 controls processing body formation. *eLife* **5**, e18746 doi: 10.7554/eLife.18746 (2016).

G. Nawaz, H. Kang. Rice OsRH58, a chloroplast DEAD-box helicase, improves salt or drought stress tolerance in Arabidopsis by affecting chloroplast translation. *BMC Plant Biol.* **19**, 17 (2019).

D. L. Nelson, H. T. Orr, S. T. Warren. The unstable repeats—three evolving faces of neurodegenerative disease. *Neuron* **77**, 825-43 (2013).

L. V. Nguyen, H. Y. Seok, D. H. Woo, S. Y. Lee, Y. H. Moon. Overexpression of the DEAD-box helicase gene AtRH17 confers tolerance to salt stress in *Arabidopsis*. *Int. J. Mol. Sci.* **19**, E3777 doi: 10.3390/ijms19123777 (2018).

S. Phadtare, K. Severinov. RNA remodeling and gene regulation by cold shock proteins. *RNA* **7**, 788-95 (2018).

S. U. Pickering. Emulsions. *J. Chem. Soc., Trans.* **91**, 2001-2021 (1907).

F. Pir Cakmak, C. D. Keating. Combining Catalytic Microparticles with Droplets Formed by Phase Coexistence: Adsorption and Activity of Natural Clays at the Aqueous/Aqueous Interface. *Sci. Rep.* **7**, 3215 (2017).

D. S. W. Protter, R. Parker. Principles and Properties of Stress Granules. *Trends Cell Biol.* **26**, 668-679 (2016).

E. Renella, T. Sára, M. Juen, C. Wunderlich, L. Imbert, Z. Solyom, A. Favier, I. Ayala, K. Weinhäupl, P. Schanda, R. Konrat, C. Kreutz, B. Brutcsher. RNA binding and chaperone activity of the E. coli cold shock protein CspA. *Nucleic Acids Res.* **45**, 4255-4268 (2017).

N. D. Sen, F. Zhou, M. S. Harris, N. T. Ingolia, A. G. Hinnebusch. eIF4B stimulates translation of long RNAs with structured 5' UTRs and low closed-loop potential but weak dependence on eIF4G. *Proc. Natl. Acad. Sci. USA* **113**, 10464-72 (2016).

U. Sheth, R. Parker. P Bodies and the Control of mRNA Translation and Degradation. *Mol. Cell* **25**, 635-646 (2007).

Y. Shin, C. P. Brangwynne. Liquid phase condensation in cell physiology and disease. *Science* **357**, eaaf4382 doi: 10.1126/science.aaf4382 (2017).

T. Trcek, M. Grosch, A. York, H. Schroff, T. Lionnet, R. Lehmann. Drosophila germ granules are structured and contain homotypic mRNA clusters. *Nat. Commun.* **6**, 7962 (2015).

B. Van Treeck, R. Parker. Emerging Roles for Intermolecular RNA-RNA Interactions in RNP Assemblies. *Cell* **174**, 791-802 (2018).

B. Van Treeck, D. S. W. Protter, T. Matheny, A. Khong, C. D. Link, R. Parker. RNA self-assembly contributes to stress granule formation and defining the stress granule transcriptome. *Proc. Natl. Acad. Sci. USA* **115**, 2734-2739 (2018).

J. R. Vieregg, M. Lueckheide, A. M. Marciel, L. Leon, A. J. Bologna, J. R. Rivera, M. V. Tirrell. Oligonucleotide-peptide complexes: phase control by hybridization. *J. Am. Chem. Soc.* **140**, 1642-1648 (2018).

J. A. West, M. Mito, S. Kurosaka, T. Takumi, C. Tanegashima, T. Chujo, K. Yanaka, R. E. Kingston, T. Hirose, C. Bond, A. Fox, S. Nakagawa. Structural, super-resolution microscopy analysis of paraspeckle nuclear body organization. *J. Cell Biol.* **214**, 817-30 (2016).

Y. Xing, R. Yao, Y. Zhang, C. Guo, S. Jiang, G. Xu, R. Dong, L. Yang. *SLERT* Regulates DDX21 Rings Associated with Pol I Transcription. *Cell* **169**, 664-678 (2017).

Y. Yang, Z. Fang, X. Chen, W. Zhang, Y. Xie, Y. Chen, Z. Liu, W. Yuan. An Overview of Pickering Emulsions: Solid-Particle Materials, Classification, Morphology, and Applications. *Front. Pharmacol.* **8**, 287 (2017).

Y. M. Yevdokimov, S. G. Skuridin, G. B. Lortkipanidze. Liquid-crystalline dispersions of nucleic acids. *Liquid Crystals* **12**, 1-16 (1992).

G. Zanchetta, T. Bellini, M. Nakata, N. A. Clark. Physical polymerization and liquid crystallization of RNA oligomers. *J. Am. Chem. Soc.* **130**, 12864-5 (2008).

M. Zhu, G. Chen, T. Dong, L. Wang, J. Zhang, Z. Zhao, Z. Hu. SIDEAD21, a Putative DEAD-Box Helicase Gene, Regulates Salt and Drought Tolerance and Stress-Related Genes in Tomato. *PLoS One* **10**, e0133849 doi: 10.1371/journal.pone.0133849 (2015).

Supplemental Material

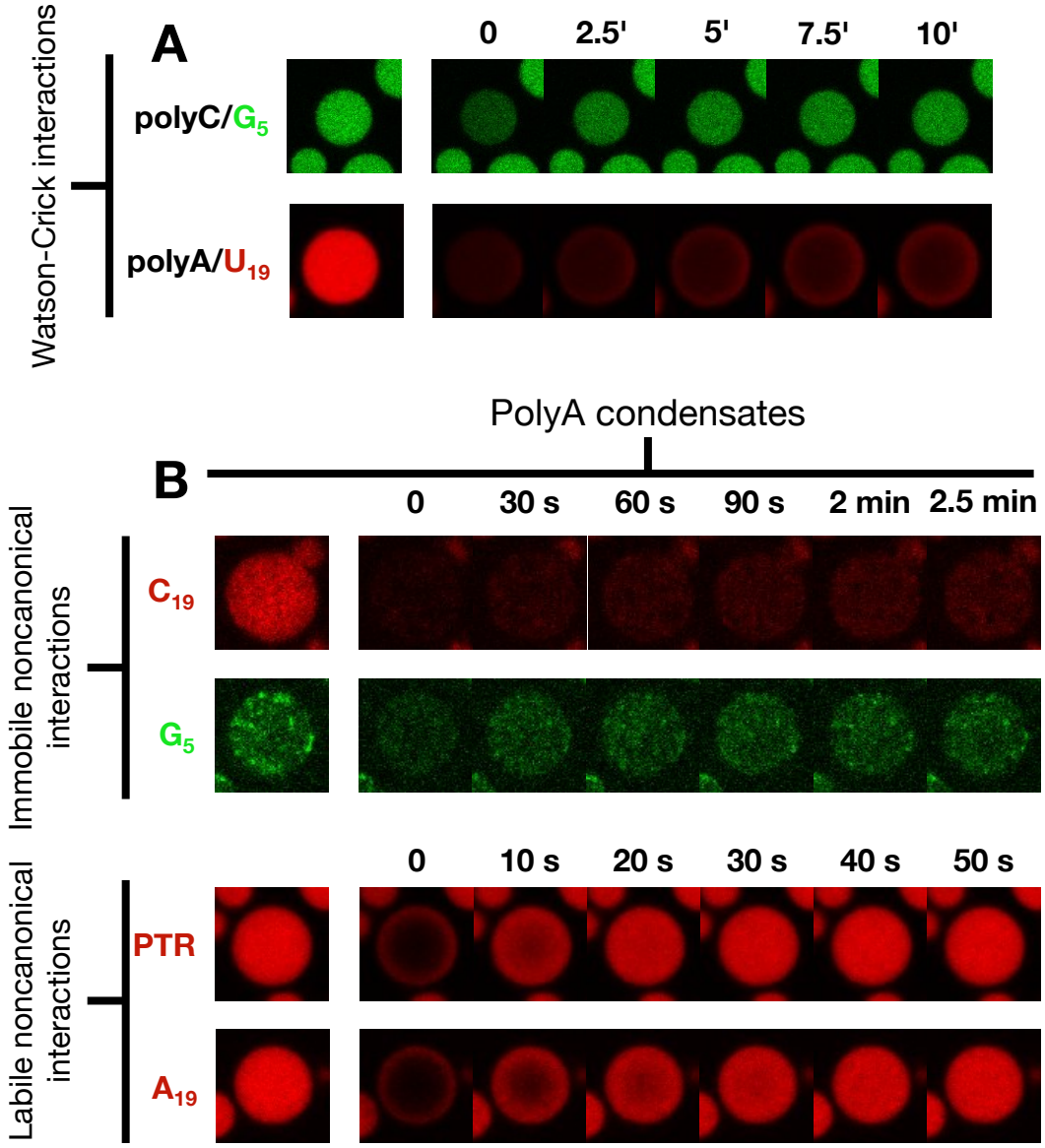

Figure S1. Related to Figure 1. Timelapse microscopy tracking recovery post-photobleaching in pairwise scaffold/oligo combinations. **(A)** Watson-Crick interactions coincide with slow recovery kinetics. **(B)** Noncanonical interactions are observed to be in two categories, immobile interactions (above) and labile interactions (below).

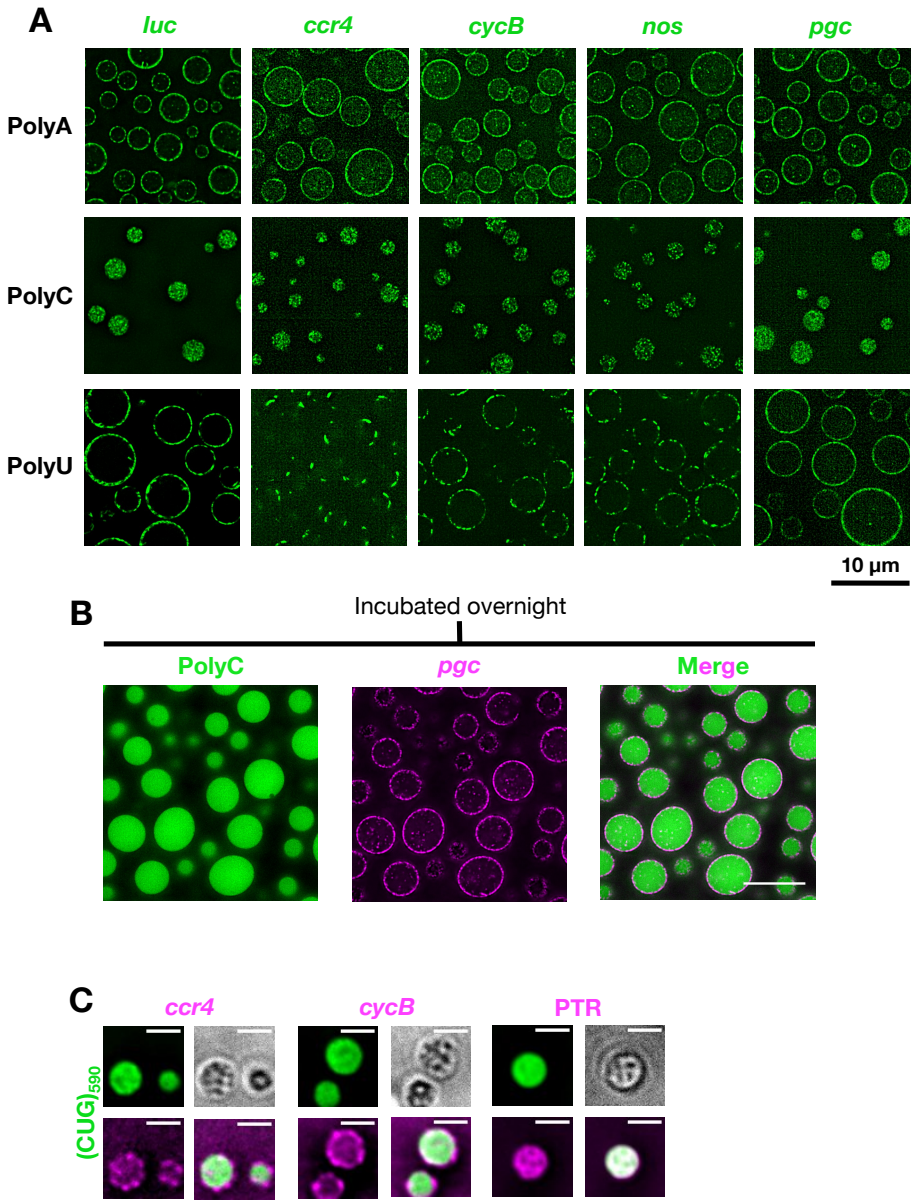

Figure S2. Related to Figure 3. RNA self-assemblies recruit *in vitro* transcribed RNAs to their surfaces. **(A)** Homopolymers were condensed with the indicated fluorescent *in* vitro transcribed RNA and incubated 1-2 hours before imaging. PolyA and polyU assemblies demonstrate robust surface recruitment of many different RNAs. By contrast, all RNAs are internalized in polyC assemblies. **(B)** PolyC was condensed with fluorescent *pgc* and labeled with fluorescent G_5, then incubated overnight before imaging. In contrast to the earlier timepoint, polyC now demonstrates robust surface recruitment of RNA. Scale bar is 15 µm. **(C)** CUG reRNA foci recruit other RNAs. Similarly to *luc*, *ccr4* and *cycB* are recruited into punctate structures on the foci surfaces. In contrast, PTR is internalized. Scale bars are 3 µm.